PAPER

Check for updates

Enhanced adsorption capacity and selectivity towards strontium ions in aqueous systems by sulfonation of CO_2 derived porous carbon†

S. Baik,[a] H. Zhang, [ID][b] Y. K. Kim,[a] D. Harbottle*[b] and J. W. Lee [ID]*[a]

Oxygen-enriched carbon materials derived from carbon dioxide were functionalized using sulfonic acid to remove Sr^{2+} ions from aqueous solutions. Synthesized sulfonated porous carbon materials (PC-SO_3H) showed higher adsorption capacity and selectivity towards Sr^{2+} than non-functionalized porous carbons (PC). The formation of the C-SO_3H functional group in PC-SO_3H and its ability to proton exchange with Sr^{2+} was the main contributor to the enhanced performance. The maximum uptake capacity of Sr^{2+} by PC-SO_3H was 18.97 mg g^{-1}, which was 1.74 times greater than PC. PC-SO_3H removed 99.9% and 97.6% of Sr^{2+} from aqueous solutions with initial Sr^{2+} concentrations of 5 mg L^{-1} and 10 mg L^{-1}, respectively. Sr^{2+} adsorption showed rapid kinetics, reaching the adsorption equilibrium within 1 h with high adsorption capacity at equilibrium which is 3.52 times greater than that of PC. Additionally, PC-SO_3H selectively adsorbed Sr^{2+} even in the presence of excess amounts of competing ions. Sulfonation of oxygen-enriched carbon had a significant effect on enhancing the affinity towards Sr^{2+} and suppressing adsorption towards other competing ions.

Introduction

Nuclear power is considered a promising candidate to satisfy the increased demand for energy. Currently nuclear power accounts for 4.8% of the world's total energy supply, and the proportion of energy supplied by nuclear is anticipated to grow.[1,2] However, radioactive waste from nuclear power can cause long-term environmental and health threats. In particular, ^{89}Sr and ^{90}Sr are radioactive isotopes which are present in nuclear reactors and various forms of nuclear waste,[3] and if released into the environment (*e.g.* nuclear incidents such as Chernobyl and Fukushima), ^{89}Sr and ^{90}Sr can present a significant public health risk following exposure to the radioactivity.[4,5] Furthermore, strontium exhibits a long half-life (28.8 years) and a high decay energy; therefore effective ways to treat strontium (Sr^{2+}) contaminated environments must be considered.[6]

Adsorption is often considered a feasible and somewhat economical method for the recovery of radioactive isotopes from liquid wastes.[7–10] Numerous studies have considered the removal of Sr^{2+} from aqueous environments using various adsorbents. Clay minerals such as kaolinite[11] and attapulgite[12]

were frequently studied due to its large edge surface and high ability for ion exchange which is common and effective mechanism for adsorption in aqueous systems.[13,14] Along with the ability for ion exchange, the porous structure is usually favored when designing effective adsorbents.[15–17] Therefore, studies moves onto various materials with those characteristics such as zeolite,[18] silica,[19,20] titanosilicate,[21] Prussian blue,[22] and titanate nanotubes.[23]

While carbon exhibits the right physical properties along with low cost and its abundance, removal performance of Sr^{2+} is poor with carbon-based adsorbents exhibiting low removal efficiencies below 70% (ref. 24–26) and low selectivity for Sr^{2+}.[27,28] Research to improve the adsorption properties of carbon-based materials, especially the removal of Sr^{2+}, has been limited but is the focus of this study.

In the current study, carbon dioxide (CO_2)-derived porous carbon materials have been functionalized with sulfonic acid to enhance removal of Sr^{2+}. The sulfonic acid groups have been identified to improve the removal efficiency of heavy metal ions such as cadmium,[29] lead[30] and uranium,[31] but there is no evidence relating to strontium adsorption. Recently, Aguila *et al.*[32] reported a metal organic framework (MOF)-SO_3H for the removal of Sr^{2+}. The authors suggested the possibility of cation exchange between the proton in SO_3H and Sr^{2+}, but experimental confirmation of this hypothesis was not provided. To the best of our knowledge, this is the first study to confirm the effect of SO_3H functional group for improved Sr^{2+} removal from aqueous systems. The reaction to functionalize the carbon backbone with SO_3H groups is demonstrated and

[a]Department of Chemical and Biomolecular Engineering, Korea Advanced Institute of Science and Technology (KAIST), 291 Daehak-ro (373-1 Guseong-dong), Yuseong-gu, Daejeon 34141, Republic of Korea. E-mail: jaewlee@kaist.ac.kr

[b]School of Chemical and Process Engineering, University of Leeds, Leeds LS2 9JT, UK. E-mail: D.Harbottle@leeds.ac.uk

† Electronic supplementary information (ESI) available: SEM images, BET measurements details. See DOI: 10.1039/c7ra09541d

supplemented with detailed material characterization. Various comparative adsorption studies between the sulfonated porous carbon and non-functionalized porous carbon were investigated to highlight the performance characteristics of SO_3H groups, specifically Sr^{2+} adsorption, with the mechanism for ion exchange clearly demonstrated and discussed.

Experimental

1.   Materials

Sodium borohydride ($NaBH_4$, >96%), hydrochloric acid (HCl, 37 wt%), strontium standard solution (1000 mg L^{-1}, for AAS), sodium chloride (NaCl, >99%) and seawater whose cations composition was 10 409 ppm Na^+, 359 ppm K^+, 1327 ppm Mg^{2+} and 176 ppm Ca^{2+} (ref. 33) were purchased from Sigma-Aldrich. Concentrated sulfuric acid (H_2SO_4, 95–98%) and potassium chloride (KCl, 99.9%) were obtained from Fluka. CO_2 used to prepare the carbon particles and acetylene and N_2O (>99.8%) for the atomic adsorption spectrometry were supplied by BOC gas. All chemicals were used without further purification. Ultrapure Milli-Q water (distilled water, DIW) with a resistivity of 18.2 MΩ cm was used in all experiments.

2.   Preparation of porous carbon (PC) from CO_2

The procedure to form the CO_2-derived porous carbon was adopted from earlier studies.[34–37] 5 g of $NaBH_4$ powder was loaded into a steel-alloy tube and the tube was placed inside the furnace (MTF 12/25/400, Carbolite Gero Ltd.). The powder was heated to 500 °C from room temperature at a heating rate of 5 °C min^{-1}. The sample was then held at this temperature for 2 h, before natural convection cooling to room temperature under a continuous flow of CO_2 at 100 mL min^{-1}. The solid product (CO_2-derived porous carbon (PC)) was then washed with 1 M HCl at 50 °C for 30 min while stirring the suspension at 300 rpm to remove any unreacted $NaBH_4$ and other impurities. The product was washed with DIW for 15 min and filtered. The wash and filtration processes were repeated further five times until the pH of the wash water was above pH 5.5. Finally, the product underwent 15 min washing in ethanol before evaporating the ethanol in air for 6 h at 100 °C.

3.   Attachment of sulfonic acid functional group to porous carbon (PC-SO₃H)

1 g of the prepared PC was dispersed in 20 mL of H_2SO_4. The mixture was heated to 130 °C in an oil bath and held at a constant temperature for 15 h while gently stirring the suspension at 200 rpm using a magnetic stirrer. Following the hydrothermal treatment the sample was cooled to room temperature and diluted in DIW and then filtered using filter paper (grade 1). Following the filtration the product was washed with DIW for 15 min and subsequently filtered. The wash and filtration processes using DIW were once again repeated until the pH exceeded 5. Finally, the product (sulfonated porous carbon (PC-SO₃H)) was air dried for 24 h at 120 °C.

4.   Characterization

Elemental analysis was conducted using a CHNS/O elemental analyzer (Thermo Fisher Scientific, Flash 2000). Fourier transform infrared (FTIR) spectra were collected using the Thermo Fisher Scientific Nicolet iS10 with an attenuated total reflection (ATR) accessory. X-ray photoelectron spectroscopy (XPS) data were acquired using a multi-purpose XPS device (Thermo Fisher Scientific, Sigma Probe) equipped with an MXR1 gun (400 μm). Scanning electron microscopy (SEM) images and energy dispersive spectroscopy (EDS) data were obtained using a field emission SEM (FEI Company, Magellan 400). Prior to the measurement (XPS and SEM) the powder samples were deposited onto a carbon tape. The nitrogen adsorption/desorption isotherms at 77 K were obtained using a Micromeritics 3Flex. The surface area for PC and PC-SO₃H was calculated according to the Brunauer–Emmett–Teller (BET) method, and the pore size distribution was determined from a non-local density functional theory (NLDFT) method.

5.   Strontium adsorption experiments

To determine the equilibrium adsorption capacity of the formed products, a Sr^{2+} adsorption isotherm was constructed by measuring the Sr^{2+} uptake at a range of initial Sr^{2+} concentrations. The initial Sr^{2+} concentrations (1, 5, 10, 20, 50, 100, 200 and 350 mg L^{-1}) were determined by diluting a stock solution (1000 mg L^{-1}) using DIW. 20 mg of the powdered sample was added to 20 mL of each Sr^{2+} solution (solid to liquid ratio = 1 g L^{-1}), and the suspension was shaken for 24 h at room temperature using an orbital shaker.

For the adsorption kinetic test the initial Sr^{2+} concentration was fixed at 20 mg L^{-1} and the suspension (1 g L^{-1}) was shaken at room temperature for 0.17, 0.33, 0.66, 1, 2, 3 and 5 h. For both isotherm and kinetic studies, following Sr^{2+} adsorption, the suspension was centrifuged at 11 000 rpm for 15 min and the supernatant was recovered and filtered using a 0.45 μm syringe filter. The Sr^{2+} concentration remaining in the supernatant was quantified using a fast sequential atomic absorption spectrometer (AAS, VARIAN AA240FS).

Results & discussion

1.   Structural analysis for synthesized PC-SO₃H

The chemical composition of the synthesized PC-SO₃H measured by elemental analyzer (EA) is shown in Table 1. Sulfur and oxygen contents were shown to increase following the sulfonation of PC even though the observed sulfur composition is a bit lower than its expected value. This suggests that the sulfonic acid groups are chemically bound to the carbon surface in the PC-SO₃H as intended.

Attachment of the sulfonic acid groups to the PC was verified from the FTIR spectra as shown in Fig. 1. The peak at 550 cm^{-1} can be assigned to the C–S stretch[38] and the peak at 1059 cm^{-1} corresponds to the SO_3^- stretch.[39] Peaks at 1154 cm^{-1} and 1200 cm^{-1} confirm the existence of SO_2 related bonds while the peaks are slightly shifted (higher wave numbers) when compared to the literature values.[40,41] This shift was also

Table 1 Chemical compositions of PC and PC-SO$_3$H measured by the elemental analyzer (CHNS/O)

	PC		PC-SO$_3$H	
	Expected[a]	Observed	Expected[a]	Observed
C	74%	76.89%	65.26%	65.73%
H	2%	2.51%	0.21%	2.13%
N	—	0.20%	0.17%	0.19%
S	—	—	6.82%	1.77%
O	17%	15.44%	23.33%	25.93%

[a] The expected chemical composition of PC is averaged value from previous studies,[34,37] and that of PC-SO$_3$H is determined based on the assumption that 10% of C–H bonds in PC are replaced by C-SO$_3$H bonds.
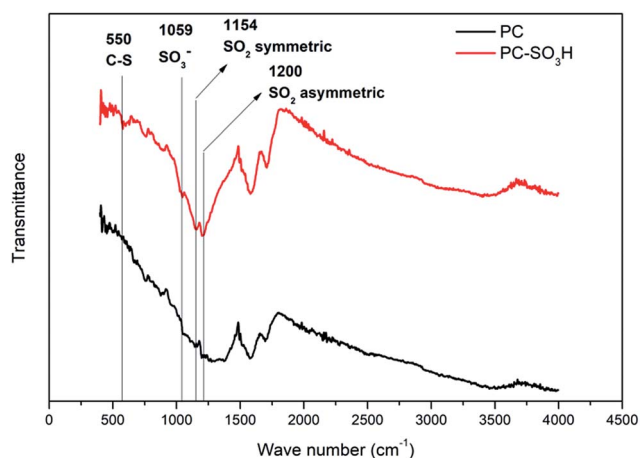

Fig. 1 FTIR spectra and peak assignments of PC-SO$_3$H including PC as reference.

Fig. 2 XPS spectra of C 1s peaks for (a) PC and (b) PC-SO$_3$H, respectively; and O 1s peaks for (c) PC and (d) PC-SO$_3$H.

reported from the previous studies for sulfonic acid-treated carbon materials.[38,42] The remaining peaks in the spectra can be assigned to either C–O or C–B, which are observed in both PC and PC-SO$_3$H samples that are synthesized from CO$_2$.[35–37] It should be noted that the presence of both C–S and S–O bonds in PC-SO$_3$H but the absence in PC indicate the successful chemical bonding of sulfonic acid group to the carbon in PC-SO$_3$H.

The surface elemental composition of the two samples was confirmed by XPS. From the data, PC contained 82.93% carbon, 13.74% oxygen and 3.34% boron, with the composition changing to 78.36% carbon, 17.54% oxygen, 1.84% boron and 2.26% sulfur for PC-SO$_3$H. In good agreement with the elemental compositions shown in Table 1, the sulfonation of PC increased both the oxygen and sulfur content in PC-SO$_3$H. The slight increase in sulfur content when measured by XPS compared to EA suggests that the sulfur atoms are enriched on the surface of carbon. To better understand the nature of the chemical bonds in PC and PC-SO$_3$H, deconvolution of the C 1s, O 1s, S 2p and B 1s spectra was conducted. As shown in the C 1s spectra of PC (Fig. 2(a)), the three peaks can be assigned to C=C (283.6 eV), C–C (285.2 eV) and C=O (288.5 eV),[43–48] while the additional peak observed in the C 1s spectra of PC-SO$_3$H
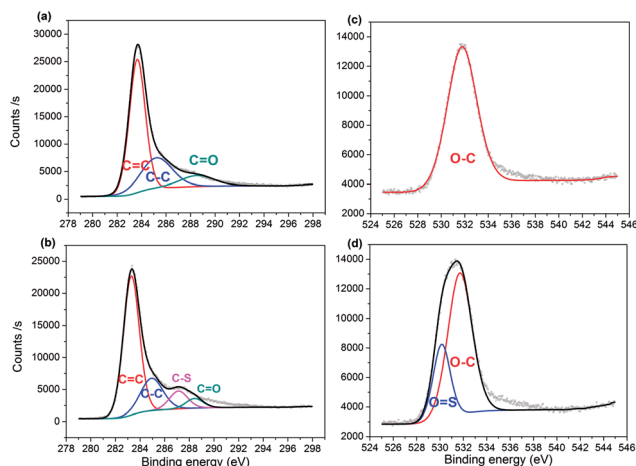
(Fig. 2(b)) corresponds to C–S bonds (287.1 eV).[44,46,49] Deconvolution of the O 1s spectra is shown in Fig. 2(c) and (d). A main peak centered at 531.7 eV is attributed to the O–C group, and a second peak observed for PC-SO$_3$H can be assigned to O=S bonds.[46,47] The C–S and O=S bonds of the PC-SO$_3$H can be clearly identified through the deconvolution of the XPS spectra (Fig. 2(b) and (d)). Moreover, for PC-SO$_3$H (Fig. 3(b)) the S 2p peak centered at 167.4 eV corresponds to C–S–O bonds,[43,45,50] which is absent for PC. Deconvolution of the B 1s spectra confirmed no changes following the sulfonation step, as shown in Fig. 3(c) and (d). As such, it is reasonable to state that the sulfur atoms bind to the carbon and oxygen atoms and not the boron atoms. Hence, the majority of the sulfur exists in the form of C–S–O, which is present in the C-SO$_3$H functional group.

Chemical composition and elemental mapping was determined by SEM-EDS (Fig. 4 and S1†). For PC-SO$_3$H the composition profile (Fig. 4(a)) was shown to be 69.73% carbon, 26.33%
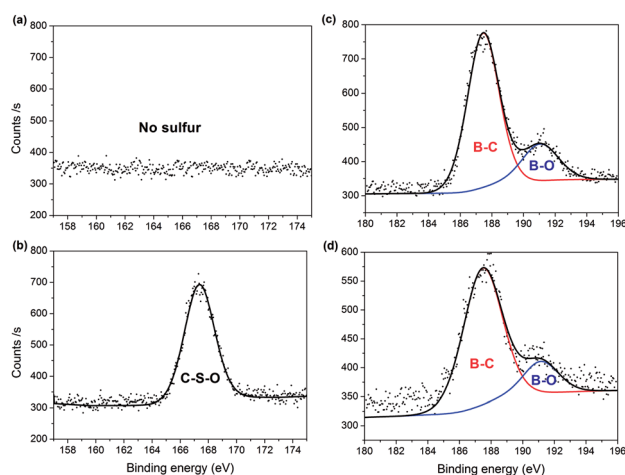

Fig. 3 XPS spectra showing: absence and presence of S 2p peaks in (a) PC and (b) PC-SO$_3$H, respectively; and B 1s peaks for (c) PC and (d) PC-SO$_3$H.
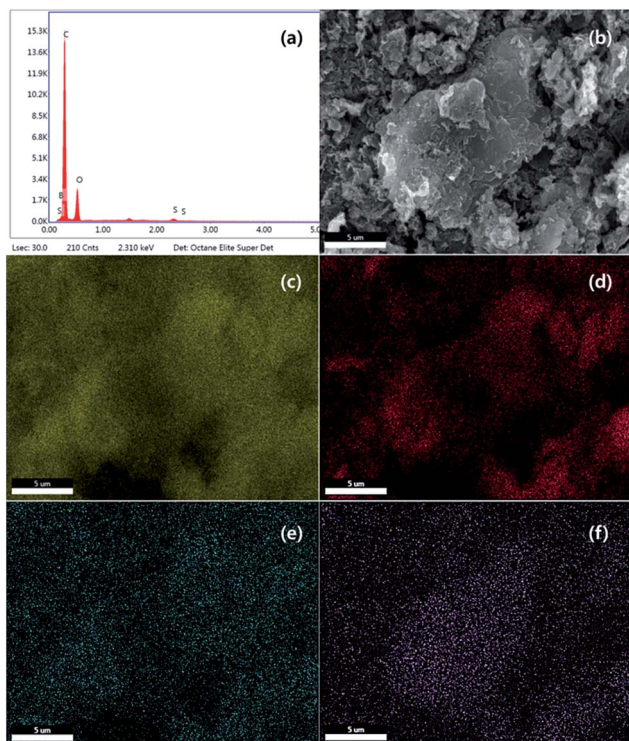
Fig. 4   SEM-EDS (a) composition profile, (b) image, (c) carbon map, (d) oxygen map, (e) boron map and (f) sulfur map for PC-SO$_3$H.

oxygen, 1.39% boron and 2.56% sulfur, which is in excellent agreement with the composition determined by EA shown in Table 1. Elemental maps in Fig. 4(b–f) show that all atoms including sulfur are uniformly distributed and dispersed across the carbon surface. Although PC-SO$_3$H shows porous morphology similar to PC in SEM images (Fig. S1†), the specific BET surface area decreased after sulfonation (Table S1†). Both isotherm curve and pore size distribution (Fig. S2†) indicate the collapse of pores by sulfuric acid, which may be the reason why specific surface area was reduced.

2.   Strontium ion adsorption

The Sr^{2+} adsorption capacity of PC and PC-SO$_3$H was determined by fitting the equilibrium adsorption data to the Langmuir-isotherm model:

$$Q_e = \frac{Q_m b C_e}{1 + b C_e} \tag{1}$$

where Q_e (mg g^{-1}) is the equilibrium adsorption, Q_m (mg g^{-1}) is the theoretical maximum adsorption capacity, b (L mg^{-1}) is the Langmuir constant which represents the affinity between Sr^{2+} and the adsorbent, and C_e (mg L^{-1}) is the ionic concentration at equilibrium. Fig. 5 shows the amount of Sr^{2+} adsorbed as a function of the equilibrium concentration, with the data fitted using eqn (1). It shows good agreement between the experimental data and the Langmuir model for both PC and PC-SO$_3$H. Based on the isotherm fitting parameters (Table 2), the maximum adsorption capacity of PC-SO$_3$H is 1.74 times higher
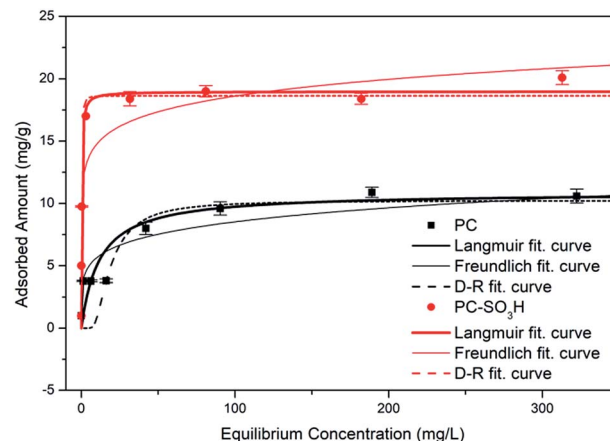

Fig. 5   Adsorption isotherms of Sr^{2+} onto PC and PC-SO$_3$H with fitted Langmuir, Freundlich, and Dubinin–Radushkevich isotherm curves.

Table 2   Isotherm parameters for Langmuir, Freundlich and Dubinin–Radushkevich models

		PC	PC-SO$_3$H
Langmuir	Q_m	10.89 mg g^{-1}	18.97 mg g^{-1}
	b	0.085 L mg^{-1}	4.399 L mg^{-1}
	R^2	0.995	0.990
Freundlich	K_F	3.73 L mg^{-1}	11.69 L mg^{-1}
	N_F	5.07	9.89
	R^2	0.923	0.757
Dubinin–Radushkevich	Q_m	10.24 mg g^{-1}	18.64 mg g^{-1}
	β	4.57×10^{-5} mol^2 J^{-2}	8.92×10^{-9} mol^2 J^{-2}
	R^2	0.972	0.959
	E	0.11 kJ mol^{-1}	7.49 kJ mol^{-1}

than PC. Moreover, the larger b value of PC-SO$_3$H than PC indicates the higher affinity of sulfonic acid group toward Sr^{2+}. Therefore, addition of sulfonic acid groups onto the carbon backbone provides a positive contribution to the adsorption of Sr^{2+}.

Other isotherm models were tested to fit the data as well, but Langmuir isotherm showed the highest accordance based on R^2 value. Freundlich isotherm curve was fitted with the equation defined as

$$Q_e = K_F C_e^{1/N_F} \tag{2}$$

where K_F (L mg^{-1}) and N_F (–) are the Freundlich constants which indicate an approximate ability of adsorption.

The Dubinin–Radushkevich (D–R) curve was fitted with the equation

$$Q_e = Q_m \exp(-\beta \varepsilon^2) \tag{3}$$

where Q_e (mg g^{-1}) is the equilibrium adsorption, Q_m (mg g^{-1}) is the theoretical maximum adsorption, β (mol^2 J^{-2}) is the D–R isotherm coefficient related to mean free energy and ε is the D–R isotherm constant, which can be calculated by following equation:

$$\varepsilon = RT \ln\left(1 + \frac{1}{C_e}\right) \quad (4)$$

where R is the gas constant (8.314 J mol^{-1} K^{-1}), and T is the absolute temperature (K). The mean free energy E (J mol^{-1}), which is an indicator for the type of a sorption process, can be calculated using the following relationship.

$$E = \frac{1}{\sqrt{2\beta}} \quad (5)$$

As both PC and PC-SO$_3$H have the E value smaller than 8 kJ mol^{-1}, physical adsorption may be the dominant mechanism. However, the E value of PC-SO$_3$H is close to 8 kJ mol^{-1}, which indicates adsorption also occurred in terms of ion exchange.[51,52]

The improved adsorption capacity of PC-SO$_3$H is attributed to the ion exchange between Sr^{2+} and the proton in SO$_3$H. To validate this mechanism the exchanged amount of ions was confirmed by measuring the pH of the Sr^{2+} solution following the adsorption test. As shown in Fig. 6, the proton concentration per gram of PC-SO$_3$H increased with the increasing concentration of Sr^{2+}. For 100 and 350 mg L^{-1} Sr^{2+} solutions, 0.42 and 0.62 mmol g^{-1} of protons were exchanged, respectively. These values appear reasonable considering that the adsorbed amount of Sr^{2+} from initial solution concentrations of 100 and 350 mg L^{-1} equalled 0.22 mmol g^{-1} and 0.25 mmol g^{-1}, respectively. These data not only support the mechanism of Sr^{2+} removal by ion exchange with the proton in PC-SO$_3$H, but also quantify the exchange ratio of proton to Sr^{2+} to be approximately 2.

Ion exchange between Sr^{2+} and proton was confirmed in XPS results as well. The clear peak shift was observed in comparison between O 1s spectra of pristine PC-SO$_3$H and Sr^{2+}-adsorbed PC-SO$_3$H (Fig. S3(a)†). This shift is caused by the replacement of H$^+$ into Sr^{2+} which is bonded to oxygen atoms. In addition, Sr 3d peaks obtained from PC-SO$_3$H after adsorption (Fig. S3(b)†)

show peak shift compared to element Sr. That is due to the bond between Sr and electronegative moiety of oxygen.

The enhanced Sr^{2+} adsorption performance of the synthesized PC-SO$_3$H was compared to previously reported values for carbon-based adsorbents. As shown in Table 3, PC-SO$_3$H exhibits outstanding or equivalent performance among carbon-based adsorbents including CNTs and graphenes which often require complex synthesis routes. As such, sulfonation of carbon materials is a viable facile method to produce economical adsorbents for Sr^{2+}.

Furthermore, the Sr^{2+} removal efficiency from aqueous solutions of low Sr^{2+} concentration is an important performance parameter when evaluating adsorbents, since these often represent conditions encountered in the environment. Sr^{2+} removal efficiencies of PC and PC-SO$_3$H from aqueous solutions containing 5 mg L^{-1} and 10 mg L^{-1} Sr^{2+} are shown in Table 4. For 5 mg L^{-1} Sr^{2+} solution, the removal efficiencies were 99.9% and 75.6% for PC-SO$_3$H and PC, respectively. These efficiencies reduced to 97.6% and 37.8% when the particles were dispersed in 10 mg L^{-1} Sr^{2+} solution. Hence, the data demonstrates the high removal efficiency of PC-SO$_3$H when adsorbing trace amounts of Sr^{2+} in aqueous solutions.

The distribution coefficient (K_d, mL g^{-1}), which represents the affinity between Sr^{2+} and adsorbent, is another indicator to verify the performance of adsorbents. K_d is calculated as follows:

$$K_d = \frac{(C_0 - C_e)}{C_e}\left(\frac{V}{m}\right) \quad (6)$$

where C_0 and C_e (mg L^{-1}) are the initial and equilibrium concentrations of Sr^{2+}, V (mL) is the volume of solution and m (g) is the weight of adsorbents. The calculated K_d values shown in Table 4 demonstrate that PC-SO$_3$H has a much higher affinity toward Sr^{2+} than PC. Typically, the K_d value on the order of 10^4 or 10^5 is judged as an excellent level.[54,55] Thus, the calculated K_d value of 4.07 × 10^4 mL g^{-1} for PC-SO$_3$H demonstrated a much higher selectivity toward Sr^{2+} than PC.

Normally removal efficiency of ions is affected by the pH of liquid. Therefore confirmation of adsorbents' performance in various pH conditions is important to ensure their applicability in industry. PC-SO$_3$H was tested with the initial solution of varying pH conditions from 2 to 12. As show in Fig. 7, PC-SO$_3$H
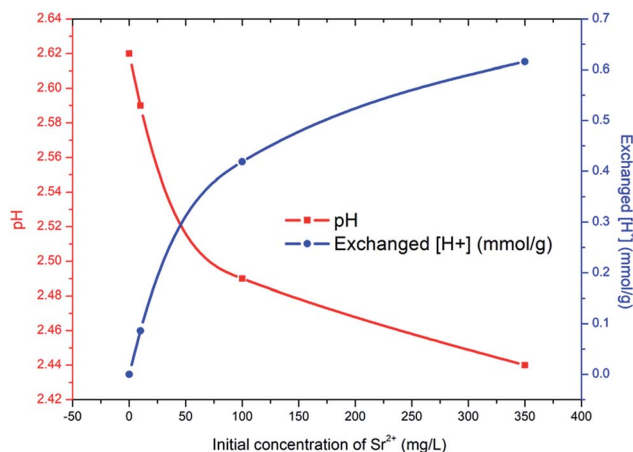

Fig. 6 Measured pH (red line and square symbol) and exchanged amount of proton per gram of PC-SO$_3$H (blue line and circle symbol) of Sr^{2+} solutions with the initial concentrations of 0, 10, 100 and 350 mg L^{-1}.

Table 3 Comparison of adsorption capacity of PC-SO$_3$H with other carbon-based adsorbents

Materials	Adsorption capacity^a (mg g^{-1})
PC-SO$_3$H	18.97 (this work)
Oxidatively modified carbon	0.48 (ref. 24)
Multi-walled CNT/iron oxide	9.18 (ref. 25)
Graphene oxide	23.66 (ref. 26)
Activated carbon	12.11 (ref. 27)
MWCNTs–SMP hybrids	14.92 (ref. 53)
Oxidized MWCNTs	10.87 (ref. 53)

^{a} Theoretical maximum Sr^{2+} adsorption capacity calculated by the Langmuir isotherm model.

Table 4   Removal efficiency and K_d values for PC and PC–SO$_3$H

	PC	PC–SO$_3$H
Removal efficiency at 5 mg L^{-1}	75.6%	99.9%
Removal efficiency at 10 mg L^{-1}	37.8%	97.6%
K_d at 10 mg L^{-1} (mL g^{-1})	6.08×10^2 mL g^{-1}	4.07×10^4 mL g^{-1}

shows high removal efficiency both in acidic (pH 4) as well as basic conditions (pH 10). However, it shows reduced adsorption performance in extreme acidic media with pH 2. On the other hands, adsorption capacity was increased by 99% in extremely basic solution with pH 12. That may be because the mechanism for the adsorption of PC–SO$_3$H is based on ion exchange between proton and strontium, which may be hindered in acidic conditions and promoted in basic conditions.

Along with the removal efficiency the Sr^{2+} adsorption kinetics, more specifically the initial adsorption rate, is an important performance parameter. The adsorption kinetics of both carbon-based adsorbents was quantified using the following pseudo-second-order kinetics model:

$$\frac{t}{Q_t} = \frac{1}{k_2 Q_e^2} + \frac{t}{Q_e} \qquad (7)$$

where Q_t (mg g^{-1}) is the amount of Sr^{2+} adsorbed at time t (min), Q_e (mg g^{-1}) is the amount of Sr^{2+} adsorbed at equilibrium, and k_2 (g (mg^{-1} min^{-1})) is the rate constant. Each particle sample was dispersed in 20 mg L^{-1} Sr^{2+} solution at a particle concentration of 1 g L^{-1}. The suspension was shaken and samples periodically removed, and the concentration of Sr^{2+} normalized to initial concentration is shown in Fig. 8. The fitting parameters, Q_e and k_2, of the pseudo-second-order rate equation are shown in Table 5. PC–SO$_3$H exhibits a higher rate constant k_2, indicating rapid adsorption when compared to PC, along with an equilibrium adsorption capacity which is 3.52 times greater than PC.
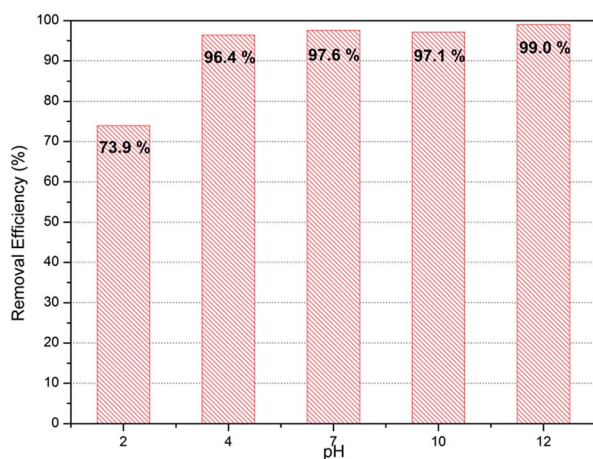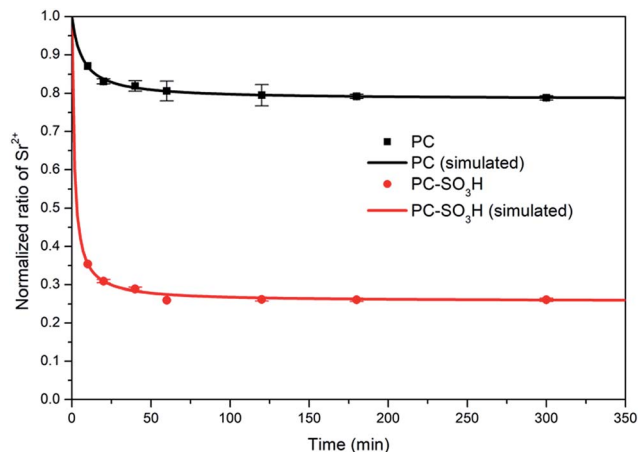

Fig. 8   Normalized ratio of Sr^{2+} ($C_0 = 20$ mg L^{-1}) as a function of time. Lines represent the fits of the pseudo-second order rate equation.

As demonstrated, the sulfonic acid groups of PC–SO$_3$H promote the enhancement of Sr^{2+} removal performance (adsorption kinetics and capacity) when compared to PC. Moreover, the sulfonic acid groups improve the selectivity of the carbon-based adsorbent for trace amounts of Sr^{2+} when in the presence of excess competing ions, see Fig. 9. When dispersed in seawater PC–SO$_3$H removed 49.24% of Sr^{2+} from seawater having 10 mg L^{-1} Sr^{2+} (Fig. 9(a)). Although the adsorption efficiency from seawater is much lower than pure water condition (97.6% for 10 mg L^{-1} Sr^{2+}) due to the blocking effect caused by excess amount of other competing ions, however, PC removed only 13.37% of Sr^{2+} under the same condition. It should be noted that PC–SO$_3$H is much more effective at removing Sr^{2+} from complex ionic solutions such as seawater. To better understand the effect of competing ions, a model solution consisting of 10 mg L^{-1} Sr^{2+}, 400 mg L^{-1} K$^+$, 10 000 mg L^{-1} Na$^+$, 200 mg L^{-1} Ca^{2+} and 1300 mg L^{-1} Mg^{2+} was used to re-evaluate the effect of competing ions. Compared to the Sr^{2+} adsorption from the Sr^{2+} diluted solution, the adsorption of Na$^+$, K$^+$ and Mg^{2+} is nearly negligible. Interestingly, removal efficiencies of PC–SO$_3$H towards K$^+$, Na$^+$ and Mg^{2+} were even reduced compared to those of PC as shown in Fig. 9(b). It means that sulfonation not only improves the affinity towards Sr^{2+}, but also inhibits the adsorption of competing ions at the same time. Especially for Na$^+$, which accounts for the biggest part of cations in seawater, sulfonation in PC–SO$_3$H can reduce Na removal by about 1/30 compared to the PC case. Bivalent Sr^{2+} can be more selectively bound to the sulfonic acid sites than monovalent

Fig. 7   Sr^{2+} removal efficiency of PC–SO$_3$H in various pH conditions (C_0 for Sr^{2+} = 10 mg L^{-1}).

Table 5   Kinetic parameters for fitting pseudo-second-order kinetics curves

	PC	PC–SO$_3$H
Q_e	4.317 mg g^{-1}	15.195 mg g^{-1}
k_2	0.03532 g (mg^{-1} min^{-1})	0.0444 g (mg^{-1} min^{-1})
R^2	0.9938	0.9861
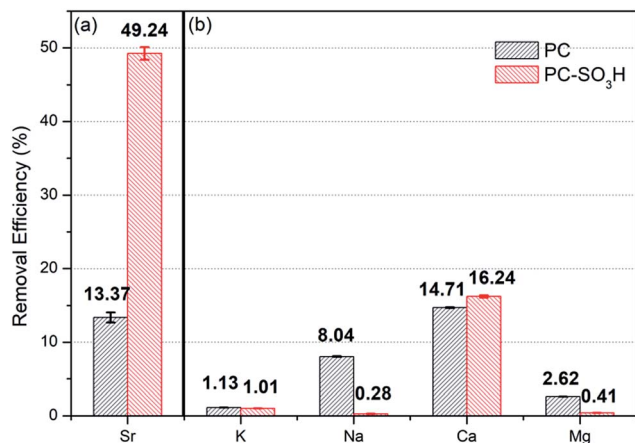
Fig. 9 Removal efficiency of (a) Sr^{2+} in seawater and (b) competitive ions (K^+, Na^+, Ca^{2+} and Mg^{2+}) in model solution ($C_0 = 400$ mg L^{-1} for K, 10 000 mg L^{-1} for Na, 200 mg L^{-1} for Ca and 1300 mg L^{-1} for Mg) for PC and PC-SO_3H.

Na^+. That is an encouraging result and the functionalization of carbon with sulfonic acid group is an effective way for the selective removal of Sr^{2+} in contaminated water.

Conclusions

We have introduced a facile method to functionalize CO_2-derived porous carbon materials with SO_3H group for the Sr^{2+} removal in aqueous solutions. Due to the ion exchange between the proton in SO_3H group and Sr^{2+} in the solution, synthesized PC-SO_3H shows enhanced Sr^{2+} adsorption performance in terms of removal capacity, selectivity and kinetics. In addition, PC-SO_3H provides outstanding selectivity towards Sr^{2+} even in aqueous solutions with excess amounts of competing ions though its exact mechanism is still needed to be studied. This work suggests a potential of functionalized carbons as adsorbents to remove the traced amounts of Sr^{2+} ions in contaminated water with nuclear wastes.

Conflicts of interest

There are no conflicts to declare.

Acknowledgements

Notes and references

1 I. E. Agecy, *Key world energy statistics*, International Energy Agecy, 2016.

2 Y. Kim, Y. K. Kim, S. Kim, D. Harbottle and J. W. Lee, *Chem. Eng. J.*, 2017, **313**, 1042–1050.

3 S. Chegrouche, A. Mellah and M. Barkat, *Desalination*, 2009, **235**, 306–318.

4 B. O. Boehm, S. Rosinger, D. Belyi and J. W. Dietrich, *N. Engl. J. Med.*, 2011, **365**, 676–678.

5 Y. K. Kim, Y. Kim, S. Kim, D. Harbottle and J. W. Lee, *J. Environ. Chem. Eng.*, 2017, **5**, 975–986.

6 A. Ahmadpour, M. Zabihi, M. Tahmasbi and T. R. Bastami, *J. Hazard. Mater.*, 2010, **182**, 552–556.

7 A. Shahzad, W. Miran, K. Rasool, M. Nawaz, J. Jang, S.-R. Lim and D. S. Lee, *RSC Adv.*, 2017, **7**, 9764–9771.

8 M. R. Awual, T. Yaita, T. Taguchi, H. Shiwaku, S. Suzuki and Y. Okamoto, *J. Hazard. Mater.*, 2014, **278**, 227–235.

9 H.-M. Yang, S.-C. Jang, S. B. Hong, K.-W. Lee, C. Roh, Y. S. Huh and B.-K. Seo, *J. Alloys Compd.*, 2016, **657**, 387–393.

10 H. Yang, L. Sun, J. Zhai, H. Li, Y. Zhao and H. Yu, *J. Mater. Chem. A*, 2014, **2**, 326–332.

11 Z. Ning, M. Ishiguro, L. K. Koopal, T. Sato and J. i. Kashiwagi, *Soil Sci. Plant Nutr.*, 2017, **63**, 14–17.

12 D. Liu and H. Zheng, *J. Radioanal. Nucl. Chem.*, 2017, **311**, 1883–1890.

13 B. Yıldız, H. N. Erten and M. Kış, *J. Radioanal. Nucl. Chem.*, 2011, **288**, 475–483.

14 H. Zhang, Y. K. Kim, T. N. Hunter, A. P. Brown, J. W. Lee and D. Harbottle, *J. Mater. Chem. A*, 2017, **5**, 15130–15143.

15 Y. F. Jia, B. Xiao and K. M. Thomas, *Langmuir*, 2002, **18**, 470–478.

16 S. Biniak, M. Pakuła, G. S. Szymański and A. Świątkowski, *Langmuir*, 1999, **15**, 6117–6122.

17 X. Mao, Z. Yan, T. Sheng, M. Gao, H. Zhu, W. Xiao and D. Wang, *Carbon*, 2017, **111**, 162–172.

18 Y. Zhang, X. Lin, S. Hu, X. Zhang and X. Luo, *RSC Adv.*, 2016, **6**, 73959–73973.

19 Y. Song, H. Ou, W. Bian, Y. Zhang, J. Pan, Y. Liu and W. Huang, *J. Inorg. Organomet. Polym. Mater.*, 2013, **23**, 1325–1334.

20 A. Y. Zhang, E. Kuraoka and M. Kumagai, *Sep. Purif. Technol.*, 2006, **50**, 35–44.

21 H. Liu, A. Yonezawa, K. Kumagai, M. Sano and T. Miyake, *J. Mater. Chem. A*, 2015, **3**, 1562–1568.

22 T. Li, F. He and Y. Dai, *J. Radioanal. Nucl. Chem.*, 2016, **310**, 1139–1145.

23 L. K. Dhandole, J. Ryu, J.-M. Lim, B.-T. Oh, J. H. Park, B.-G. Kim and J. S. Jang, *RSC Adv.*, 2016, **6**, 98449–98456.

24 A. Khannanov, V. V. Nekljudov, B. Gareev, A. Kiiamov, J. M. Tour and A. M. Dimiev, *Carbon*, 2017, **115**, 394–401.

25 C. Chen, J. Hu, D. Shao, J. Li and X. Wang, *J. Hazard. Mater.*, 2009, **164**, 923–928.

26 A. Y. Romanchuk, A. S. Slesarev, S. N. Kalmykov, D. V. Kosynkin and J. M. Tour, *Phys. Chem. Chem. Phys.*, 2013, **15**, 2321–2327.

27 E. Kaçan and C. Kütahyalı, *J. Anal. Appl. Pyrolysis*, 2012, **97**, 149–157.

28 A. Y. Romanchuk, A. S. Kuzenkova, A. S. Slesarev, J. M. Tour and S. N. Kalmykov, *Solvent Extr. Ion Exch.*, 2016, **34**, 594–602.

29 E. W. Shin and R. M. Rowell, *Chemosphere*, 2005, **60**, 1054–1061.

30 V. V. Kulkarni, A. K. Golder and P. K. Ghosh, *RSC Adv.*, 2016, **6**, 5341–5349.

31 Z.-B. Zhang, X.-F. Yu, X.-H. Cao, R. Hua, M. Li and Y.-H. Liu, *J. Radioanal. Nucl. Chem.*, 2014, **301**, 821–830.

32 B. Aguila, D. Banerjee, Z. Nie, Y. Shin, S. Ma and P. K. Thallapally, *Chem. Commun.*, 2016, **52**, 5940–5942.

33 Y. K. Kim, T. Kim, Y. Kim, D. Harbottle and J. W. Lee, *J. Hazard. Mater.*, 2017, **340**, 130–139.

34 J. Zhang and J. W. Lee, *Carbon*, 2013, **53**, 216–221.

35 A. Byeon, J. Park, S. Baik, Y. Jung and J. W. Lee, *J. Mater. Chem. A*, 2015, **3**, 5843–5849.

36 Y. Kim, W. Lee, G. M. Kim and J. W. Lee, *RSC Adv.*, 2016, **6**, 54889–54897.

37 S. Baik, B. L. Suh, A. Byeon, J. Kim and J. W. Lee, *J. CO$_2$ Util.*, 2017, **20**, 73–80.

38 H. Yu, Y. Jin, Z. Li, F. Peng and H. Wang, *J. Solid State Chem.*, 2008, **181**, 432–438.

39 K. Nakajima and M. Hara, *ACS Catal.*, 2012, **2**, 1296–1304.

40 W. W. Mar and E. Somsook, *Procedia Eng.*, 2012, **32**, 212–218.

41 B. Xie, L. Hong, P. Chen and B. Zhu, *Polym. Bull.*, 2015, **73**, 891–908.

42 S. Madakbaş, E. Çakmakçı and M. V. Kahraman, *Thermochim. Acta*, 2013, **552**, 1–4.

43 F. Liu, J. Sun, L. Zhu, X. Meng, C. Qi and F.-S. Xiao, *J. Mater. Chem.*, 2012, **22**, 5495.

44 X. Li, S. P. Lau, L. Tang, R. Ji and P. Yang, *Nanoscale*, 2014, **6**, 5323–5328.

45 H. Huang, Y.-C. Lu, A.-J. Wang, J.-H. Liu, J.-R. Chen and J.-J. Feng, *RSC Adv.*, 2014, **4**, 11872.

46 Q. Xu, P. Pu, J. Zhao, C. Dong, C. Gao, Y. Chen, J. Chen, Y. Liu and H. Zhou, *J. Mater. Chem. A*, 2015, **3**, 542–546.

47 B. P. Vinayan, Z. Zhao-Karger, T. Diemant, V. S. Chakravadhanula, N. I. Schwarzburger, M. A. Cambaz, R. J. Behm, C. Kubel and M. Fichtner, *Nanoscale*, 2016, **8**, 3296–3306.

48 Q. Xu, Y. Liu, C. Gao, J. Wei, H. Zhou, Y. Chen, C. Dong, T. S. Sreeprasad, N. Li and Z. Xia, *J. Mater. Chem. C*, 2015, **3**, 9885–9893.

49 U. Siemeling, H. Memczak, C. Bruhn, F. Vogel, F. Trager, J. E. Baio and T. Weidner, *Dalton Trans.*, 2012, **41**, 2986–2994.

50 C. Xu, Q. Han, Y. Zhao, L. Wang, Y. Li and L. Qu, *J. Mater. Chem. A*, 2015, **3**, 1841–1846.

51 B. Ma, S. Oh, W. S. Shin and S.-J. Choi, *Desalination*, 2011, **276**, 336–346.

52 Y. Park, Y.-C. Lee, W. S. Shin and S.-J. Choi, *Chem. Eng. J.*, 2010, **162**, 685–695.

53 N. Asadollahi, R. Yavari and H. Ghanadzadeh, *J. Radioanal. Nucl. Chem.*, 2015, **303**, 2445–2455.

54 H. Yang, H. Li, J. Zhai, L. Sun, Y. Zhao and H. Yu, *Chem. Eng. J.*, 2014, **246**, 10–19.

55 J. L. Mertz, Z. H. Fard, C. D. Malliakas, M. J. Manos and M. G. Kanatzidis, *Chem. Mater.*, 2013, **25**, 2116–2127.